

Structural, Thermal and Electrical Conduction Studies on LiNiPO₄: RE (RE= La, Nd) Prepared by Polyol Method

S. Karthickprabhu¹, G. Hirankumar^{2,†}, S.Thanikaikarasan² and P.J. Sebastian^{3,*}

¹Energy Materials Research Laboratory, Department of Physics, Kalasalingam University, Krishnankoil , 626 126, India.

²Centre for Scientific and Applied Research, School of Basic Engineering and Sciences,
PSN College of Engineering and Technology, Melathediyoore, 627 152, TN, India

³Instituto de Energias Renovables-UNAM, 62580, Temixco, Morelos, Mexico.

Received: January 03, 2014, Accepted: June 29, 2014, Available online: October 03, 2014

Abstract: LiNiPO₄ and LiNiPO₄: xRE (RE = La, Nd) (x = 0.01 mol%, 0.03 mol%, 0.05 mol%, 0.07 mol%, 0.09 mol%) samples have been prepared by polyol method using 1, 2 propanediol as a polyol medium. XRD patterns have indicated that the pristine LiNiPO₄ is well crystallized with orthorhombic structure *p_{nma}* space group and structurally stable compound upon doping of rare earth metals. Functional group analyses have been carried out by FTIR spectroscopic analysis. TG analysis shows that no weight loss has been observed above 600°C for both Nd³⁺ and La³⁺ doped LiNiPO₄. The morphology of the samples was analyzed through Scanning Electron Microscopy. The conductivity of LiNiPO₄ was found to be improved by 2 orders by doping of rare earth ions. It is found that lanthanum is an excellent dopant for LiNiPO₄ than neodymium due to the formation of free ion sites which causes the enhancement of conductivity. Dielectric studies support that doping of La³⁺ is favorable for conduction compared with Nd³⁺ doping

Keywords: LiNiPO₄, Li-ion battery, electrical conductivity, dielectric properties

1. INTRODUCTION

Lithium metal phosphates (LiMPO₄ M = Fe, Mn, Co, Ni), the high energy, high voltage cathodes for lithium ion batteries with olivine structures have been received considerable attention due to their low cost production, excellent cycleability, low toxicity, environmental friendliness, good thermal and chemical stability [1-3]. These three dimensional olivine structured materials are stabilized by the covalent bonding between the oxygen ions and P⁵⁺ resulting in PO₄³⁻ tetrahedral poly-anions. It does not undergo structural changes during lithiation and delithiation [4]. Among these cathode materials, the pristine LiNiPO₄ shows high voltage vs lithium while exhibiting extremely poor electrical conductivity at ambient temperature [5]. The poor electrical conductivity of LiNiPO₄ causes miserable Li⁺ intercalation/deintercalation [6]. The electrical conductivity of these metal phosphate materials have been improved by different synthesis methods [7], transition metal doping on the lattice site [8, 9], using carbon containing precursors [9, 10] and rare earth doping [11, 12, 13]. The use of

rare earth metals in the lithium ion batteries has much significance due its eco-friendly nature. Doping of rare earth metals with phospho- olivine compounds shows higher electrical conductivity [11] and considerable electro-chemical stability during charging and discharging. It has also been found that the doping of rare earth to LiNiVO₄ can improve the electrical conductivity by 2-3 orders [12]. Doping of supervalent cations in olivine phosphate facilitates the Li-ion motion and hence the enhancement of ionic and electronic conductivity [14]. Jiezi Hu et al have showed that doping of transition /rare earth metals into LiFePO₄ enhanced the conductivity by 1-3 orders [15]. Prabu et al observed that the conductivity of LiNiPO₄ has been increased by one order due to the addition of 1 mol% europium [13]. Herle et al have found that zirconium doped LiNiPO₄ shows higher conductivity than pristine LiNiPO₄ and the increment in conductivity value is mainly associated with the formation of Ni₃P as nano phase impurity [9]. Hence, in the present investigation, it is proposed to study the effect of supervalent cations such as La³⁺ and Nd³⁺ doping on the structural and electrical properties of LiNiPO₄ at ambient temperature.

To whom correspondence should be addressed:

Email: *P.J. Sebastian: sjp@ier.unam.mx , †g.hirankumar@psnresearch.ac.in

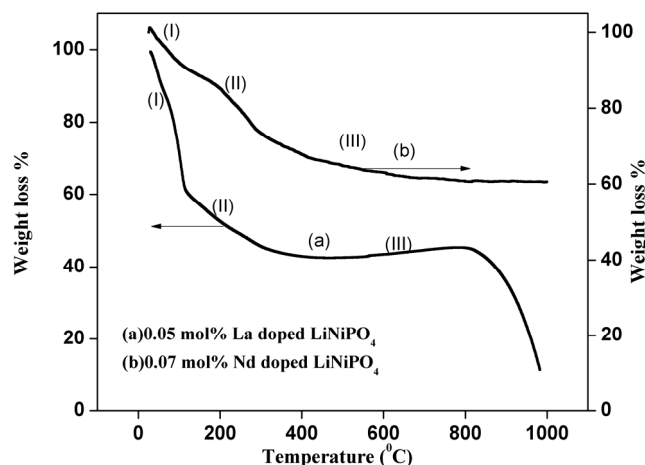


Figure 1. Thermal analysis for 0.05 mol% La^{3+} and 0.07 mol% Nd^{3+} doped LiNiPO_4

2. EXPERIMENTAL DETAILS

LiNiPO_4 : x mol RE (RE = La, Nd) ($x = 0, 0.01\%, 0.03\%, 0.05\%, 0.07\%, 0.09\%$) were prepared by polyol method. Lithium acetate ($\text{CH}_3\text{COOLi}\cdot 2\text{H}_2\text{O}$, Himedia, 99.9% Purity), Nickel acetate ($\text{Ni}(\text{O}(\text{C}=\text{O})\text{CH}_3)_2\cdot 4\text{H}_2\text{O}$, Merck with 98% purity), Ortho Phosphoric acid (H_3PO_4 , Merck), Lanthanum acetate (Himedia, 99.9% purity) and Neodymium acetate (Himedia, 99.9% purity) were used as starting materials. 1, 2 propanediol was used as polyol medium. The preparation method was already discussed elsewhere [16]. In order to get crystalline LiNiPO_4 : $x\text{RE}$, the prepared powders were calcined at 650°C for 6 hours. The prepared samples were then characterized by Exstar 6000 thermo gravimetric analyzer in the temperature range of 30°C to 1000°C with a step of $10^\circ\text{C}/\text{min}$. The XRD spectra have been recorded by XPERT-PRO x-ray diffractometer PW 3050/60 (with Cu K_α radiation) at 2θ with a step of 0.05° in the range of 10° to 80° at 25°C . FTIR studies were carried out with the aid of JASCO FT/IR-4100 fourier transform infrared spectrometer in the wave number region between 1200 and 350cm^{-1} . Morphology of the prepared powders has been identified from the JEOL-6390 type Scanning Electron Microscope. Particle size distribution measurement has been carried out by Malvern instrument at 25°C . The required amount of powder was pressed into a pellet under a pressure of 9 tons with the dimensions of 1-2 mm thickness and the diameter of 10 mm. The pellet was then sintered at 650°C for 5 hours. The pellet was sandwiched between two stainless steel electrodes, which acted as blocking electrodes. AC impedance measurements were carried out by HIOKI 3532-50 LCR HiTester at room temperature over the frequency range of 42 Hz to 1M Hz.

3. RESULTS AND DISCUSSION

3.1. Thermal Analysis

Figure 1 shows the TG curve for LiNiPO_4 : Nd and LiNiPO_4 : La precursors recorded under nitrogen atmosphere. The TG curve is represented into three regions as shown in figure 1. The first region (region I) shows an initial mass loss of and it corresponds to the

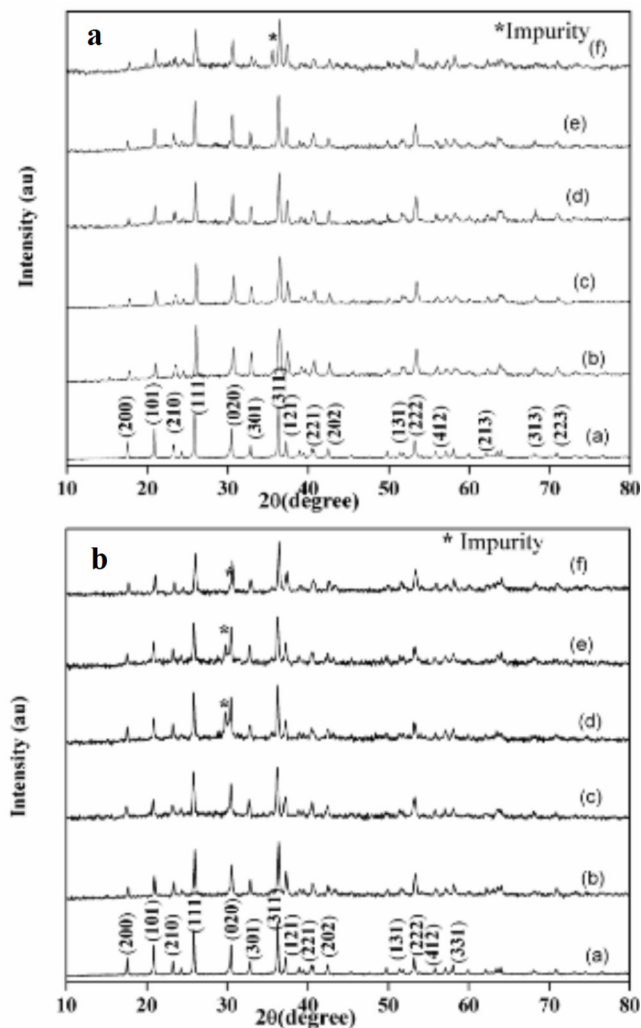


Figure 2. a: XRD patterns for LiNiPO_4 : $x\text{mol}\% \text{La}$ for different concentrations (a) $x = 0$ (b) $x = 0.01$ (c) $x = 0.03$ (d) $x = 0.05$ (e) $x = 0.07$ (f) $x = 0.09$. b: XRD patterns for LiNiPO_4 : $x\text{mol}\% \text{Nd}$ for different concentrations (a) $x = 0$ (b) $x = 0.01$ (c) $x = 0.03$ (d) $x = 0.05$ (e) $x = 0.07$ (f) $x = 0.09$.

removal of adsorbed water present in the material. The next weight loss has been noticed in the temperature range of ~ 158 - 274°C and is marked as region II. The region II is associated to the removal of propanediol and other organic residues present in the precursor. As the temperature increases beyond the region II up to 600°C (region III), the TG curve shows a weight loss of 10.14% which indicates the removal of acetate ions from the precursor [16]. There is no weight loss observed beyond the region III, which indicates that crystallization of La & Nd doped LiNiPO_4 may occur.

3.2. XRD Analysis

Figure 2a and 2b show the XRD patterns for lanthanum and neodymium doped LiNiPO_4 with different concentrations of rare earths respectively. The diffraction peaks are in full agreement with the ordered LiNiPO_4 olivine structure indexed to the orthorhombic p_{nma}

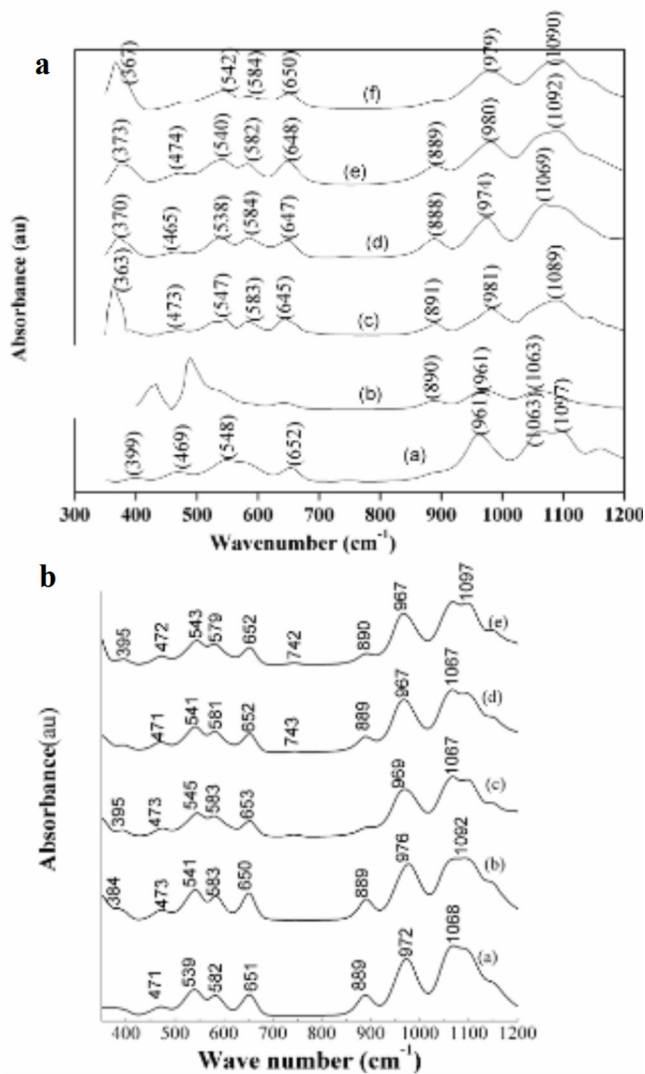


Figure 3. a: FTIR spectrum for LiNiPO_4 : xmol%La for different concentrations (a) $x = 0$ (b) $x = 0.01$ (c) $x = 0.03$ (d) $x = 0.05$ (e) $x = 0.09$. b: LiNiPO_4 : xmol%Nd for different concentrations (a) $x = 0.01$ (b) $x = 0.03$ (c) $x = 0.05$ (d) $x = 0.07$ (e) $x = 0.09$.

space group. The miller indices and "d" spacing values of all diffraction peaks of LiNiPO_4 are well matched with the JCPDS card number 01-081-1528. From the figures, it is also observed that the main diffraction peaks ((311), (111)) are shifted to higher 2θ side upon doping. The impurity peak with less intensity is only observed at $2\theta = 33.6^\circ$ in the case of 0.09mol% La doped LiNiPO_4 owing to the formation Li_3PO_4 . From the figure 2b, low concentrations (0.01 and 0.03mol%) of Nd doped samples do not show any impurity peaks while for higher concentration of neodymium, the impurity of nickel phosphate (JCPDS card number: 00-049-1082) with small intensity is noticed at $2\theta = 29.7^\circ$. Hence it is concluded that the doping of RE in LiNiPO_4 does not destruct the lattice structure of LiNiPO_4 within the concentration range studied.

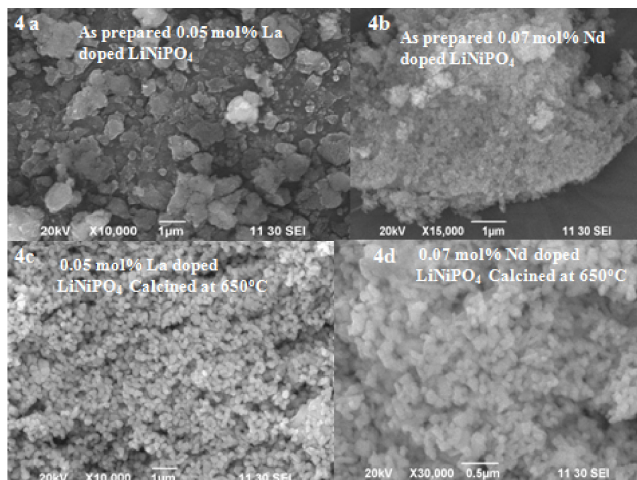


Figure 4. SEM photograph for rare earth doped LiNiPO_4 (a) As prepared 0.05 mol% La doped LiNiPO_4 (b) calcined LiNiPO_4 :0.05mol% La (c) As prepared 0.07 mol% Nd doped LiNiPO_4 (d) calcined LiNiPO_4 :0.07mol% Nd.

3.3. FTIR Analysis

The variations in the local structure and chemical bonding of the samples upon doping have been identified from FTIR spectroscopy. Figures 3a and 3b show the FTIR spectra for La^{3+} and Nd^{3+} doped LiNiPO_4 at different concentrations respectively. The bands observed in the range of 400-470 cm^{-1} (ν_2) and 570-650 cm^{-1} (ν_4) are attributed to the symmetric and antisymmetric bending mode of O-P-O bands respectively. The stretching mode of NiO_6 distorted octahedra is observed in the region of 650-653 cm^{-1} . The higher frequency vibrational band located around 969-1097 cm^{-1} imputes to the (ν_3) (PO_4) stretching mode of tetrahedral (PO_4) in LiNiPO_4 [17]. The band observed in the PO_4 stretching vibrational region of pristine LiNiPO_4 is found to be shifted to higher wavenumber side upon doping. The above results are consistent with XRD results that confirm that doping does not destruct the lattice structure and disturb the lattice parameters. Shifting of these vibrational bands implies that the doping of both Nd & La may present in the LiNiPO_4 host lattice. Similar observation has already been made in the case of vanadium doped LiCoPO_4 [18].

3.4. SEM Analysis

Figure 4a and 4b show the morphology of La doped LiNiPO_4 and Nd doped LiNiPO_4 respectively before calcinations. Both the samples show the agglomerate morphology and may be due to the presence of polyol medium. Figures 4c and 4d show the morphology of samples calcined at 650°C for 6 hrs respectively. The samples exhibit homogeneous particles with sphere like structure. The average particle size of prepared powders is found to be submicron size. Further, it is noted from the figures 4c and 4d the uniform distribution of fine particles with little agglomeration.

3.5. Particle Size Distribution Analysis

Figure 5 represents particle size distributions of pure and rare earth doped LiNiPO_4 . It is found that the size of the particles is distributed from 100 nm to 500 nm and the average particle size is

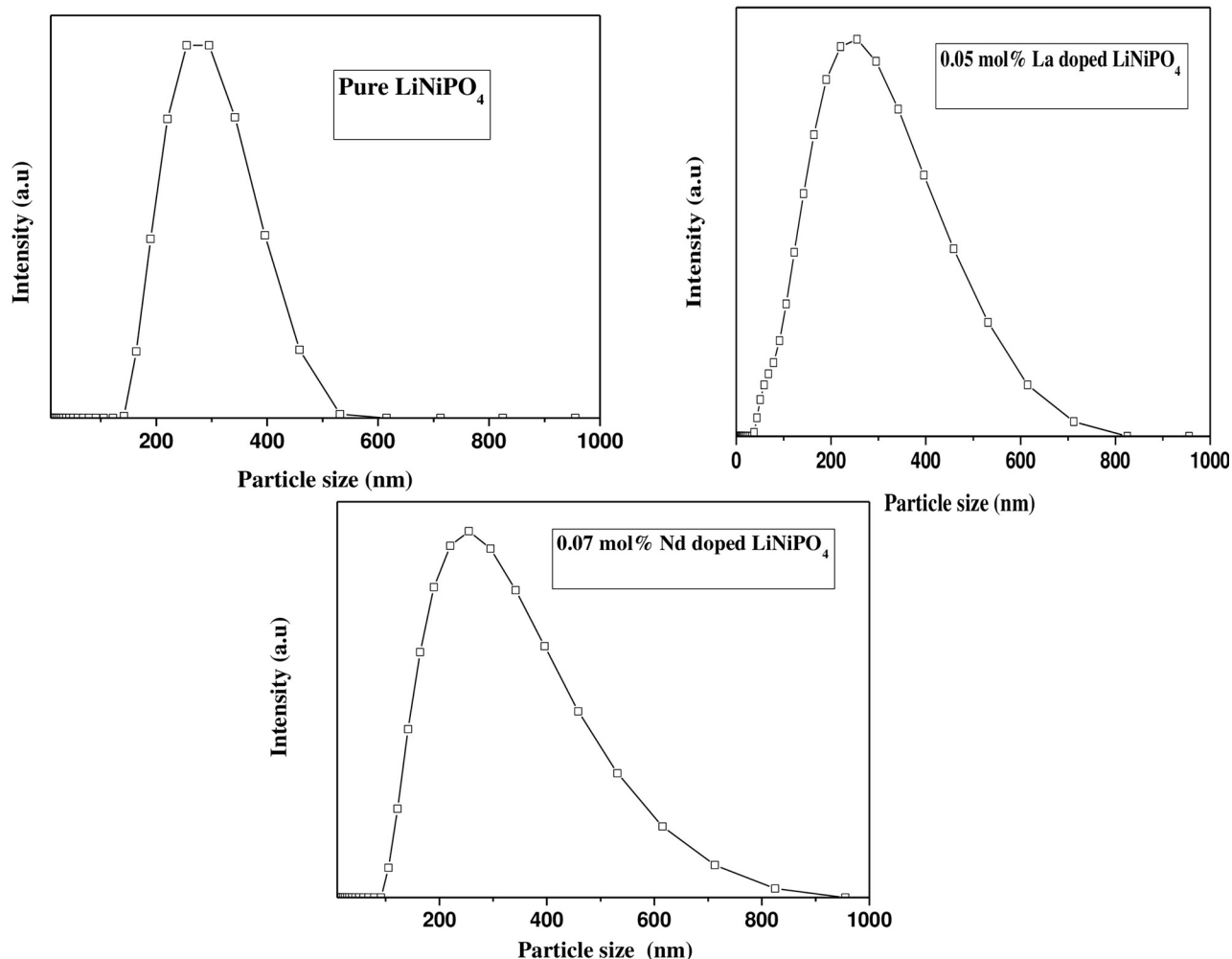


Figure 5. Particle size distributions for pure and rare earth doped LiNiPO₄.

measured as 330 nm for pure LiNiPO₄. In the case of rare earth doped samples, the particle size distribution range is measured as 180 nm-250 nm, 250 nm-290 nm for La doped and Nd doped LiNiPO₄ respectively. From the analysis, it is evident that doping of rare earth metal into LiNiPO₄ causes the reduction in the particle size of LiNiPO₄. Similar results have also been observed for La doped LiFePO₄ [11]. The average diameter (Z average d in nm) of the particles was found to be 330.4 nm, 188.9 nm, 252.8 nm for pure LiNiPO₄, La doped and Nd doped LiNiPO₄ respectively.

3.6. Impedance Analysis

Figure 6a, 6b and 6b show the cole-cole plot for pure, La and Nd doped LiNiPO₄ for different concentrations at ambient temperatures respectively. It is found that 0.05mol% La and 0.07mol% Nd doped LiNiPO₄ possess low impedance value compared to pure LiNiPO₄ and all other concentrations studied. Figure 7 represent the Cole-Cole plot (Z' versus Z'' plot) for 0.05mol% La and 0.07mol% Nd doped LiNiPO₄ at ambient temperature (fitted with Z view software) respectively. The semicircle alone has been observed for LiNiPO₄:0.07mol%Nd sample, whereas the sample LiNi-

iPO₄:0.05mol% La shows spike at low frequency region along with the depressed semicircle in the high frequency region. The bulk resistance (R_b) and capacitance values have been calculated from the Z view software and the fitted plots are presented in the figure 7. The corresponding equivalent circuit is also provided in the inset of figure 7. The equivalent circuit represents the presence of parallel combination of resistance (R_b) and constant phase element (CPE1) along with CPE2 (due to double layer capacitance) in series combination in the case of La doped sample whereas parallel combination of resistance (R_b) and CPE1 along with resistance in series. The values of capacitance are calculated as 391 pF for La³⁺ doped sample and 169 pF for Nd³⁺ doped sample, which indicate that the ion conduction process occurs through the bulk of the material. It is also noted that the center of the semicircle is lying down below the real axis i.e., the depressed semicircle, which ensures that the distribution of relaxation time and its deviates from the ideal Debye behavior [19]. From the bulk resistance (R_b) of the sample, the conductivity value has been calculated using the following relation.

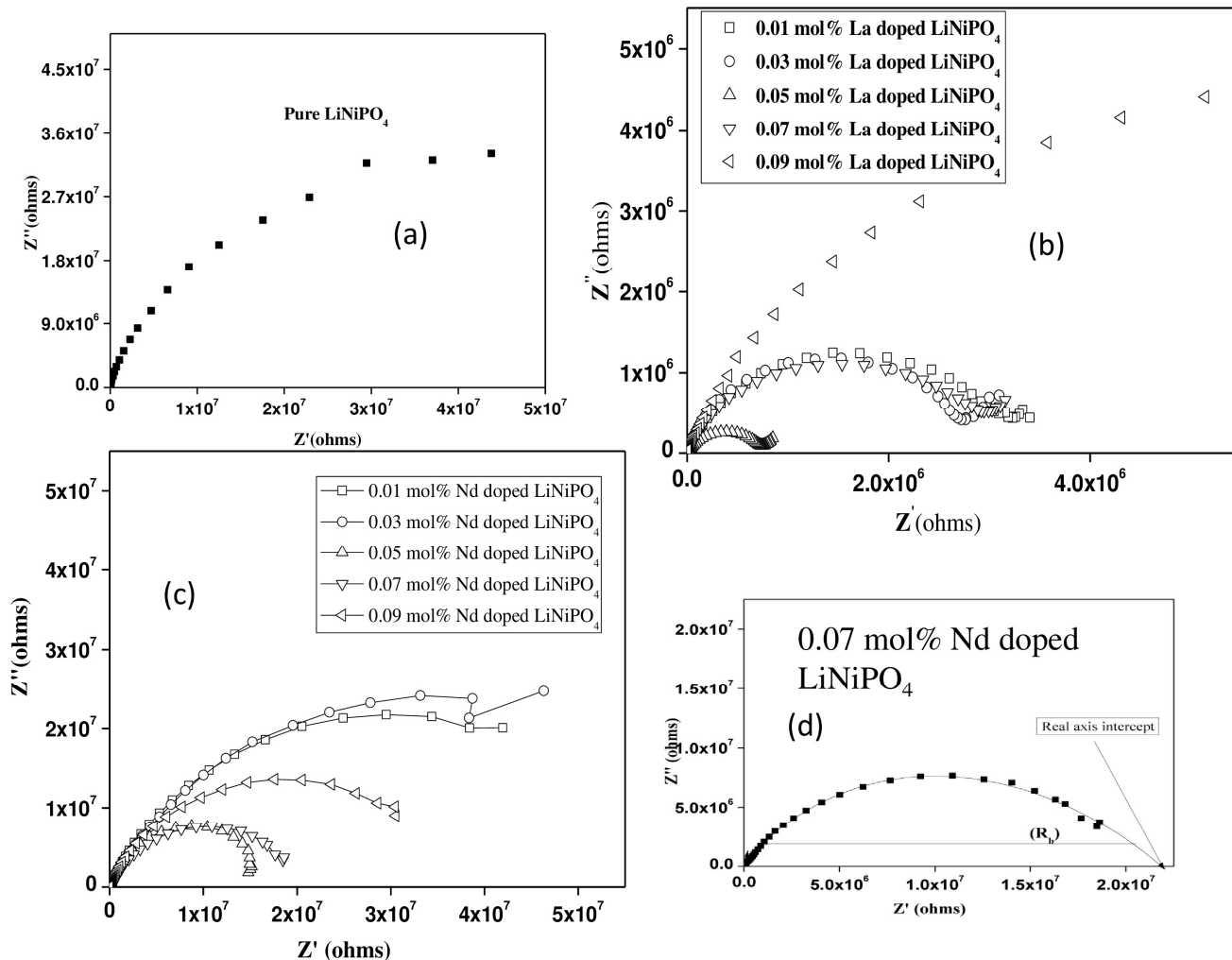


Figure 6. Cole-Cole plot for pure and rare earth doped LiNiPO_4 at different concentrations (a) Pure LiNiPO_4 (b) La doped LiNiPO_4 (c) Nd doped LiNiPO_4 .

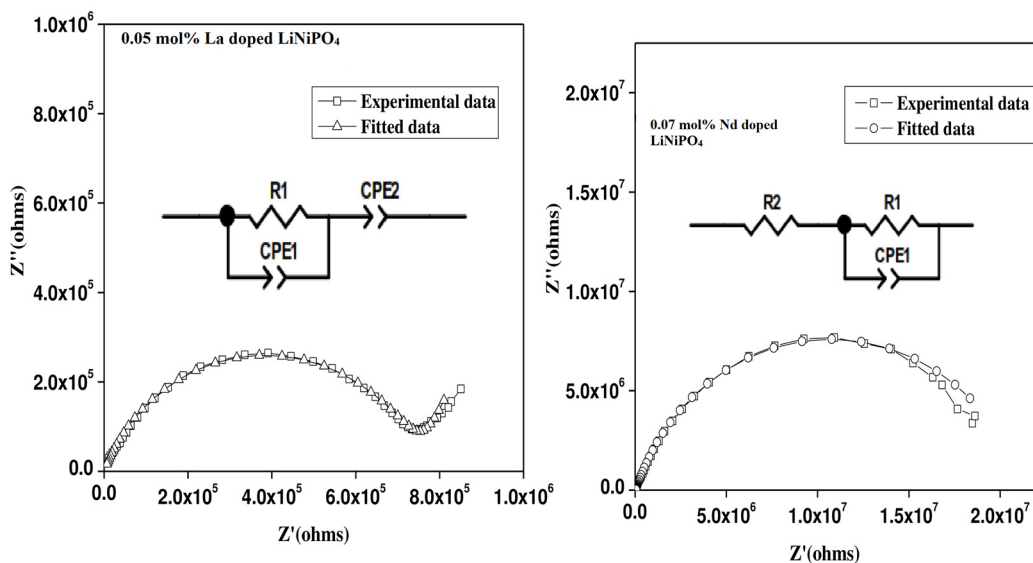


Figure 7. Equivalent circuit model for LiNiPO_4 :0.05mol%La and LiNiPO_4 :0.07%Nd

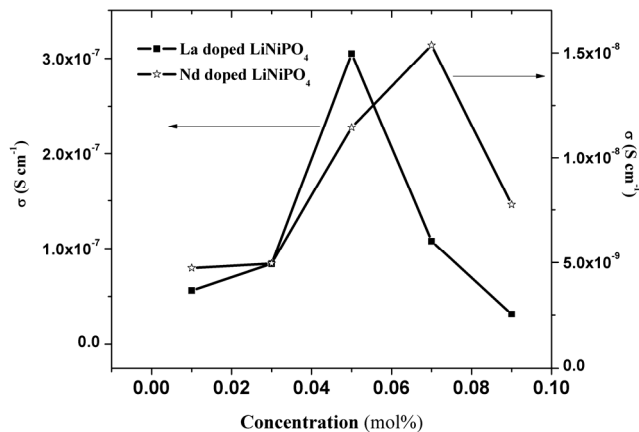


Figure 8. Concentration dependent conductivity for LiNiPO₄: xRE at ambient temperature.

$$\sigma_b = \left(\frac{1}{R_b}\right) \times \left(\frac{L}{A}\right) \tag{1}$$

where, σ_b is the bulk conductivity of the sample and L&A are thickness and area of the sample respectively. The conductivity of RE doped LiNiPO₄ is tabulated in the table 1. The maximum value of conductivity is found to be $3.05 \times 10^{-7} \text{ S cm}^{-1}$ for LiNiPO₄:0.05mol%La and $1.54 \times 10^{-8} \text{ S cm}^{-1}$ for LiNiPO₄:0.07mol%Nd at ambient temperature. The conductivity of 0.05mol% La doped LiNiPO₄ sample shows higher value than the already reported values in literature [9, 13].

3.7. Concentration Dependent of Conductivity

The variation of dc conductivity with respect to RE concentrations is shown in figure 8. For both the samples, the dc conductivity value increases upon increase of RE concentration and a maximum is reached. Further increase of RE concentration causes decrease of conductivity. The enhancement in the conductivity of the RE doped LiNiPO₄ is due to the effect of introducing the impurity bands in the electronic structure of pristine LiNiPO₄. The doping of La³⁺ and Nd³⁺ in the structure of LiNiPO₄ provides the vacant site which favors higher ion hopping rate and hence enhancement of the conductivity. Similar results have also been observed for rare earth and metal-doped LiFePO₄ [15]. Further, it has been noted that doping with polyvalent cations (La³⁺, Nd³⁺) in LiNiPO₄ could decrease

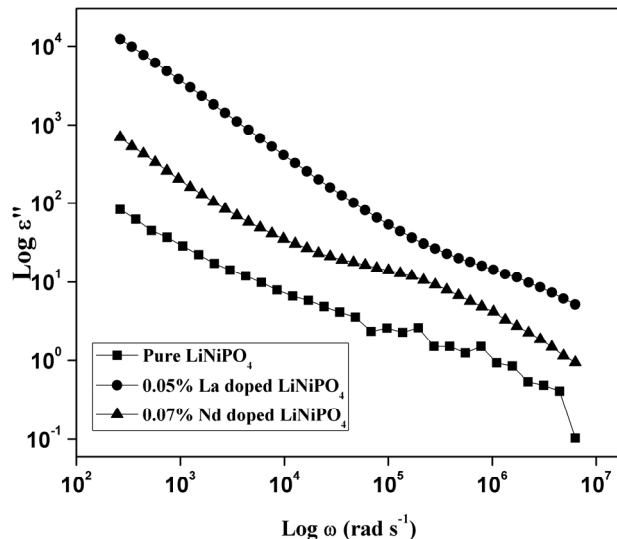


Figure 9. Dielectric loss spectra for pure and 0.05mol% La³⁺ and 0.07mol% Nd³⁺ doped LiNiPO₄.

the grain size due to cation vacancies created during charge compensation and it may increases the size of channel for Li⁺ diffusion. So, the electrical conductivity gets increased [14]. This result is consistent with the particle size distribution analysis in which the particle size gets decreased because of doping with polyvalent cations. It is also found that the 0.05mol% La³⁺ doped sample and 0.07mol% Nd³⁺ doped samples possess higher conductivity compared with other concentrations. The decrease of conductivity at higher concentration of RE may be due to the decrease of available space for the movement of ion with the excess amount of rare earth and hence blocked the migration of lithium ions that contribute to the conductivity [12].

3.8. Dielectric Analysis

The dielectric properties of any system can be characterized by frequency dependent parameters that can be defined by the complex permittivity ϵ . The complex permittivity or dielectric constant of a system is defined by

$$\epsilon = \epsilon' - j\epsilon'' \tag{2}$$

where ϵ' is real part of dielectric permittivity and ϵ'' is the dielec-

Table 1. Conductivity and “n” values for La³⁺ and Nd³⁺ doped LiNiPO₄ at ambient temperature

Concentration in mol%	La doped LiNiPO ₄ Conductivity (S cm ⁻¹)	n	Nd doped LiNiPO ₄ Conductivity (S cm ⁻¹)	n
Pure LiNiPO ₄	Above 10 ⁻⁹		-----	
0.01	5.60×10 ⁻⁸	0.09	4.74×10 ⁻⁹	0.48
0.03	8.40×10 ⁻⁸	0.07	4.95×10 ⁻⁹	0.47
0.05	3.05×10 ⁻⁷	0.06	1.15×10 ⁻⁸	0.30
0.07	1.08×10 ⁻⁷	0.10	1.54×10 ⁻⁸	0.18
0.09	3.13×10 ⁻⁸	0.24	7.75×10 ⁻⁹	0.39

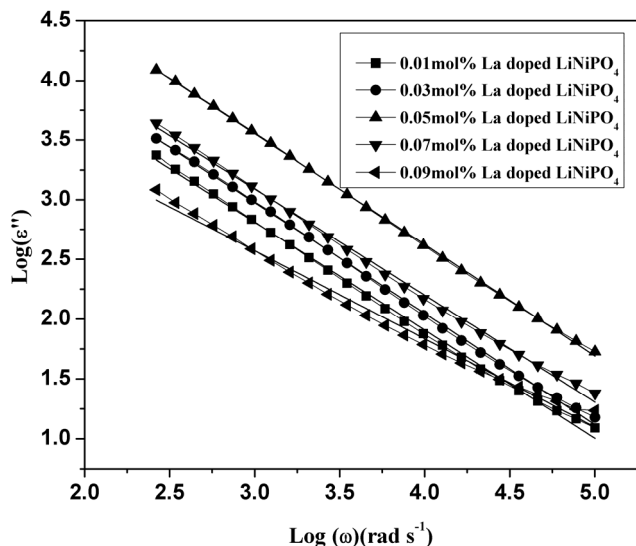


Figure 10. Logarithmic Dielectric loss spectra for La³⁺ doped LiNiPO₄ at different concentrations.

tric loss or imaginary part of dielectric permittivity. Figure 9 shows the frequency dependent of dielectric loss spectra for pure, 0.07 mol% Nd³⁺ doped and 0.05 mol% La³⁺ doped LiNiPO₄ at ambient temperature. It is observed that the magnitude of dielectric loss decreases with increase of frequencies. The dielectric loss is found to be very large at low frequency region due to free charge motion with in the material. The magnitude of dielectric loss can be regarded as the contribution of three different effects such as dc conductivity, interfacial polarization and the dipole orientation. It is also noticed from figure 9 that the higher dielectric loss value has been observed for LiNiPO₄:0.05mol%La compared with pure and Nd³⁺ doped LiNiPO₄. This can be explained on the basis of the availability of maximum number of free charge carriers within the material for motion, which contribute to the conductivity. It was already reported that the dielectric loss is directly related with the conductivity [20] of the material which is suggested by the equation $\epsilon''(\omega) = \sigma(\omega) / \omega\epsilon_0$. Figure 10 represents the variation of logarithmic dielectric loss of LiNiPO₄:xLa with respect to frequency at different concentrations of La. The plot is fitted with linear fit data with regression 0.99 and 'n' values are calculated by using the following expression [21]

$$\log(\epsilon'') = \log(A) - (1 - n) \log \omega \quad (3)$$

The calculated n values are provided in the Table 1. The contribution of dc conduction mechanism is predominant when the slope value of the plot is -1 or the 'n' value approaches zero. From the table, it is noticed that the value of 'n' is approaching zero which signifies that d.c. conduction contribution is predominant in these systems. Among the two dopants, La doped LiNiPO₄ is having the 'n' value very nearer to zero in particular 0.05mol% La doped sample that also shows higher dc conductivity. From the analysis, doping of La³⁺ in LiNiPO₄ is favorable for the enhancement of the conductivity of LiNiPO₄ compared to Nd³⁺.

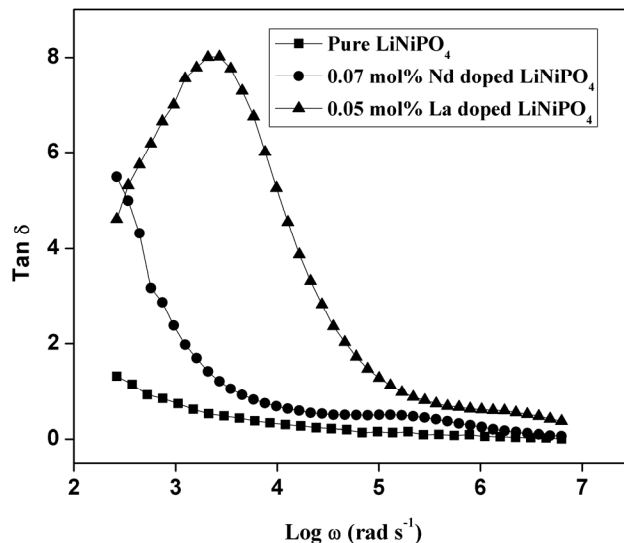


Figure 11. Dissipation factor analysis for pure and 0.05mol% La³⁺ and 0.07mol% Nd³⁺ doped LiNiPO₄.

3.9. Dissipation Factor Analysis

The dielectric loss tangent (tanδ) can be defined by the equation

$$\tan(\delta) = \frac{\epsilon''}{\epsilon'} \quad (4)$$

The variation of tanδ with respect to frequency for pure LiNiPO₄, 0.05mol% La and 0.07mol% Nd doped LiNiPO₄ samples is represented in the figure 11. The relaxation peak is observed for 0.05 mol% La doped sample that denotes the presence of relaxation mechanism in the frequency range studied. According to Sheoran [22], high loss tangent value entails higher dc conductivity for the material. In the present system, the magnitude of loss tangent is found higher for La doped sample compared to Nd doped sample and hence the conductivity. There is no appreciable relaxation peak observed in the case of Nd³⁺ sample in the frequency range studied. Hence, it is expected that LiNiPO₄: La has lesser relaxation time than Nd doped sample. The region above and below the relaxation peak frequency represent the short range motion of ions because the charge carriers are confined to potential well and ions are mobile over long distances respectively.

4. CONCLUSIONS

Lanthanum and Neodymium doped LiNiPO₄ were prepared by Polyol method using 1, 2 propanediol as polyol medium. TG/DTA analysis confirmed that the weight loss of the precursor is up to 600°C, afterwards there is no reduction in the weight. XRD analysis ensured the formation of LiNiPO₄ and impurity peak is appeared for higher concentration of dopants. FTIR analysis supported that the rare earth ions enter into the host lattice. Uniform distribution of particles with sphere like morphology has been seen for rare earth doped LiNiPO₄ from SEM analysis for the calcined samples. Particle size distribution studies also affirmed the SEM morphology studies and size of the particles is in submicron range.

LiNiPO₄:0.05mol%La has shown higher conductivity than other concentrations, pure LiNiPO₄ and LiNiPO₄: Nd at room temperature and is found to be $3.05 \times 10^{-7} \text{ S cm}^{-1}$ which is also greater than the reported value in the literature. Dielectric and $\tan \delta$ studies have also confirmed that doping of LiNiPO₄ with La³⁺ is favorable for conductivity than doping with Nd³⁺.

5. ACKNOWLEDGEMENT

The financial support from BRNS, Government of India, DAE, research project 2010/20/37P/3/BRNS/1062 is gratefully acknowledged. One of the authors (S.Karthickprabhu) thanks the BRNS, DAE, Government of India, for the award of Junior Research Fellowship.

REFERENCES

- [1] J. Wolfenstine, J. Allen, Journal of Power Sources, 136, 150 (2004).
- [2] T.R Kim, D.H. Kim, H.W. Ryu, J.H. Moon, J. Phys. Chem. Solids, 68, 1203 (2007).
- [3] C.V. Ramana, A. Ait-Salah, S. Utsunomiya, U. Becker, Chem. Mater, 18, 3788 (2006).
- [4] Thierry Drezen, Nam-Hee Kwon, Paul Bowen, Ivo Teerlinck, Motoshi Isono, Ivan Exnar, J. Power Sources, 174, 949 (2007).
- [5] K. Ressouli, K. Benkhouja, J.R. Ramos-Barrado, C. Julien, Mater. Sci and Eng. B, 98, 185 (2003).
- [6] J. Wolfenstine, J. Allen, J. Power Sources, 142, 389 (2005).
- [7] Natalia N. Bramnik, Kirill G. Bramnik, Carsten Baehtz, Helmut Ehrenberg, J. Power Sources, 145, 74 (2005).
- [8] Sung-yoon chung, Jason T. Bloking, Yet-ming Chiang, Nature Materials, 1, 123 (2002).
- [9] P. Subramaniya Herle, B. Ellis, N. Coombs, L.F. Nazar, Nature Materials, 3, 147 (2004).
- [10] J. Wolfenstine, U. Lee, B. Poesse, J.L. Allen, J. Power Sources, 144, 226 (2005).
- [11] LUO Shaohua, TIAN Yong, LI Hui, SHI Kejie, TANG Zilong, J. Rare Earths, 28, 439 (2010).
- [12] George Ting-kuo Fey, Chi-sun Wu, Pure & Appl. Chem., 69, 2329 (1997).
- [13] M. Prabu, S. Selvesekarapandian, A.R. Kulkarni, S. Karthikeyan, C. Sanjeeviraja, Trans. Nonferrous. Met. Soc. China, 22, 342 (2012).
- [14] Sathiyaraj Kandhasamy, Kalaiselvi Nallathamby, Manickam Minakshi, Progress in Solid State Chemistry, 40, 1 (2012).
- [15] Jiezi Hu, Jain Xie, Xinbing Zhao, Hongming, Xing Zhou, Gaoshao Cao, Jiangping Tu, J. Mater. Sci. Technol., 25, 405 (2009).
- [16] S. Karthickprabhu, G. Hirankumar, A. Maheswaran, R.S. Daries Bella, C. Sanjeeviraja, J. Alloys compd., 548, 65 (2013).
- [17] C.M. Julien, A. Mauger, K. Zaghbi, R. Veillette, H. Groult, Ionics, 18, 625 (2012).
- [18] A. Rajalakshmi, V.D. Nithya, K. Karthikeyan, C. Sanjeeviraja, Y.S. Lee, R. Kalai Selvan, J. Sol-Gel Sci. Technol., DOI 10.1007/s10971-012-2952-y.
- [19] A. Ben Rhaiem, F. Hlel, K. Guidara, M. Gargouri, J. Alloys Compd., 463, 440 (2008).
- [20] Hiroshi Yamamura, Saori Takeda, Katsuyoshi Kakinuma, Solid State Ionics, 178, 1059 (2007).
- [21] M. Vijayakumar, G. Hirankumar, M.S. Bhuvanewari, S. Selvasekarapandian, J. Power Sources, 117, 143 (2003).
- [22] A. Sheoran, S. Sanghi, S. Rani, A. Agarwal, V.P. Seth, J. Alloys Compd., 475, 804 (2009).